Power dissipation and time-averaged pressure in oscillating flow through a sudden area change

Barton L. Smith

Mechanical and Aerospace Engineering Department

Utah State University

Logan, Utah 84322

Gregory W. Swift

Condensed Matter and Thermal Physics Group

Los Alamos National Laboratory

Los Alamos, NM 87545

LA-UR 02-6434

Running Title: Oscillating flow through sudden area change

Abbreviated Title: Oscillating flow through a sudden area change

Abstract

Experiments on oscillating flow in a 2-D entrance/exit geometry with rounded edges are presented. It is shown that the minor losses are a function of three independent dimensionless parameters including the dimensionless edge radius. The effect of each of these parameters on the time-averaged pressure difference across the area change and acoustic power dissipation is explored by holding two parameters fixed while varying the third. Evidence is presented that the losses due to oscillatory flow in this geometry are smaller than would be expected from commonly accepted values for steady flow in similar geometry.

PACS numbers: 43.25.Qp, 43.25.Nm, 47.32.Ff, 47.60.+i

I. INTRODUCTION

When a fluid flows through a system, energy is lost to viscous dissipation effects including boundary layer turbulence and random motions in separated flows. These losses are often called head losses, since they result in a drop in pressure head along the flow path. When energy is dissipated in pipe bends, valves, expansions, entrances, or anything other than a length of straight pipe, the term "minor loss" is used.

The effects of minor losses in oscillating flow can be either detrimental or advantageous. While minor losses in steady flow are manifested by a loss of flow work (or flow energy), minor losses in oscillating flow dissipate acoustic power and create time-averaged pressure gradients. The time-averaged pressure gradient has been used to counteract streaming flows in a thermoacoustic Stirling refrigerator[1] and engine[2]. On the other hand, minor losses can result in significant power dissipation in such refrigerators and engines, and therefore may need to be minimized.

Although extensive tables[3] of losses for steady flow are available, few such data exist for oscillatory flow in any geometry, despite the fact that abrupt changes in geometry are ubiquitous in Stirling engines, thermoacoustics, and respiratory flows. Current understanding relies mostly on the assumption that the losses due to oscillatory flow can be computed by cycle averaging the losses based on steady flow data. For example, it has been assumed that the minor losses for the entrance/exit geometry in Fig. 1 are the same as for steady flow through a sudden expansion (for the outward flow) and through an entrance (for the inward flow).

Currently, at least three other research efforts are addressing oscillatory losses in sudden area changes. Wakeland and Keolian[4] have recently reported minor loss coefficients for oscillatory flow through a sharp-edged area change based on the steady-flow theory referenced below but using theoretical laminar oscillatory flow profiles. Morris *et al.*[5] are numerically studying oscillating flow in a sharp-edged two-dimensional transition with finite area ratio, while Petculescu and Wilen[6] have built an apparatus that provides very accurate

pressure/flow relationships for small flow components and have recently used this apparatus to measure the losses associated with axisymmetric acoustic diodes[7]. Knowledge of oscillating flow losses in other flow elements (pipe bends, etc.) is also necessary to minimize such losses and predict their value. In the current work, we study minor loss effects for purely oscillatory flow through a two-dimensional transition with a rounded edge and an infinite area ratio.

In steady flow through abrupt changes in geometry, minor losses and are commonly accounted for by use of a minor loss coefficient:

$$K = \frac{\rho g H}{\frac{1}{2}\rho u^2} \tag{1}$$

where H is the head loss through the component, ρ is the fluid density, g is the acceleration due to gravity, and u is the average velocity at the smallest cross-sectional area. The minor loss coefficient can be thought of as the ratio of dissipated flow energy per unit mass ($\Delta p/\rho$) to the maximum kinetic energy per unit mass in the component.

One of the few minor loss coefficients that can be theoretically determined is the "Borda-Carnot" coefficient that for steady flow through a sharp-edged expansion[8]. The common assumption of spatially uniform channel flow results in $K = 1$ for flow out of the channel into infinite space. Any departure from uniform flow results in a larger loss coefficient, as large as 1.5 for fully developed laminar channel flow. No data for flow from a rounded sudden expansion are known to the authors, although it seems to be commonly assumed that this geometry has similar losses to a sharp-edged expansion[9].

Steady entrance flow through a rounded 2-D opening has a minor loss coefficient that decreases with increasing r/h, where r is the edge radius and h is the channel width (see Fig. 1). For $r/D_h > 0.2$, where D_h is the hydraulic diameter, K becomes constant at 0.03[3]. In the current study, $r/D_h > 0.2$ for all cases.

This paper will discuss the results of an experimental study of the effects of minor losses in a rounded entrance/exit between a 2-D slot and an infinite space. The results indicate that the flow is governed by three dimensionless parameters. It will be revealed that the

exiting flow can, in some circumstances, expand considerably in the slot edges, resulting in smaller losses than those reported in steady flows. As will be discussed in Section II, calculation of minor losses from acoustic power and time-averaged pressure data requires assumptions about the behavior of time-dependent inertial effects that may not be realistic. Therefore, we will present results in terms of acoustic power dissipation and time-averaged pressure. The experimental apparatus and measurement techniques are described in Section III and a description of the results is given in Section IV.

II. TIME-AVERAGED PRESSURE AND LOSS COEFFICIENTS

Following Swift *et. al*[1], minor loss coefficients for the blowing and suction cycle are related to time-averaged pressure by writing the unsteady Bernoulli equation with losses that are assumed to be constant over each half of the cycle for flow between the points a and b in Fig. 1. It is assumed that point b is sufficiently far downstream that the velocity has become negligible. These equations are then averaged over a full cycle. During the blowing part of the cycle,

$$p_a + \frac{1}{2}\rho u_a^2 - \frac{1}{2}K_B \rho u_a^2 = p_b + \rho \int_{x_a}^{x_b} \frac{du}{dt} dx \tag{2}$$

or

$$p_a - p_b = \frac{1}{2}\rho u_a^2 (K_B - 1) + \rho \int_{x_a}^{x_b} \frac{du}{dt} dx, \tag{3}$$

where p is the time-varying pressure, K_B is the minor loss coefficient for the blowing stroke, u is the cross-stream average of the velocity, and the subscripts a and b refer to those locations in Fig. 1. Similarly, during the suction stroke,

$$p_a - p_b = -\frac{1}{2}\rho u_a^2 (K_S + 1) + \rho \int_{x_a}^{x_b} \frac{du}{dt} dx. \tag{4}$$

Averaging over a full period T,

$$\Delta P = \frac{1}{T}\int_0^{T/2} \frac{1}{2}\rho u_a^2(K_B - 1)dt - \frac{1}{T}\int_{T/2}^{T} \frac{1}{2}\rho u_a^2(K_S + 1)dt + \frac{\rho}{T}\int_0^T \left[\int_{x_a}^{x_b} \frac{du}{dt}dx\right] dt. \tag{5}$$

The form of the last (unsteady) term is not generally known and will be discussed further below. However, the integral over a cycle of the periodic function inside the brackets will go to zero and therefore this term can be ignored here. Rearranging, we have

$$\Delta P = \frac{\rho u_{a,\max}^2}{2}[(K_B - 1)\alpha_B - (K_S + 1)\alpha_S], \tag{6}$$

where

$$\begin{aligned} \alpha_B &= \frac{1}{T u_{a,\max}^2}\int_0^{T/2} u_a^2 dt, \\ \alpha_S &= \frac{1}{T u_{a,\max}^2}\int_{T/2}^{T} u_a^2 dt, \end{aligned} \tag{7}$$

ΔP is the time-averaged pressure change, and $u_{a,\max} = \max(u_a)$. If the flow is sinusoidal, then $\alpha_B = \alpha_S = 1/4$ and

$$\Delta P = \frac{\rho u_{a,\max}^2}{8}(K_B - K_S - 2). \tag{8}$$

Without a second equation, we can only gain information on the difference between the loss coefficients and cannot infer anything about them individually without additional assumptions. Swift *et. al*[1] obtained a second equation for K_B and K_S by computing dissipated acoustic power, $\dot{E} = \overline{\Delta p U}$, as a function of the loss coefficients, where the overbar indicates cycle-averaging and U is the volume flow rate. They argued that time-dependent inertial effects on pressure could be ignored since these are 90° out of phase with the volume flow rate. However, this assumption relies on the inertial pressure contribution being the same during blowing as it is during suction, which is to say that no nonlinear effects contribute to inertial pressure. This seems unlikely at high Reynolds number, and results from the present study indicate that this is not the case. The unsteady term can be computed using velocity

data acquired as described in Section III between $x = 0$ and point b. This measurement was performed for $L_o/h = 17, r/h = 1.3$, and $Re = 354$ (see definitions below). For this particular case, the difference between the magnitude of the average of the unsteady term during the outward stroke and inward stroke was on the same order as the time-averaged pressure. Hence, we cannot accurately compute K_B and K_S for such a case by using Eq. (8) and a similar equation for acoustic power dissipation ignoring the inertial term. Doing so would yield an artificially high K_B and a similarly low (and perhaps negative!) K_S . The present study also shows that the assumption of time-independent K_B and K_S is questionable. Hence, we will make only slight use of Eq. (8) here, presenting results in terms of ΔP and $\dot{E}$ instead of K_B and K_S.

Assuming that the aspect ratio of the slot is sufficiently large to ensure 2-D flow and that the axial length of the slot is not important, the time-averaged pressure and acoustic power dissipation are functions of r, h, ρ, T, $u_{a,\max}$, and the viscosity μ. Dimensional analysis shows that this flow is governed by three independent dimensionless parameters. As will be shown below, the parameter r/h affects the severity of the adverse pressure gradient experienced by the exiting flow, the Reynolds number $Re = u_{a,\max}\delta_\nu\rho/\mu$ based on the maximum velocity and the viscous penetration depth $\delta_\nu = \sqrt{\mu T/\pi\rho}$ affects turbulent transition and boundary layer thickness, and L_o/h, where $L_o = \int_0^{T/2} u_a dt$, governs the vortex pair dynamics and steady-jet tendencies.

Since it is experimentally difficult to "dial in" an exact value of L_o/h or Re, some variation is inevitable. Hence, for "fixed" cases, each of these parameters is held to within 2% of the nominal value reported.

III. EXPERIMENTAL SETUP

The apparatus used in this study is shown schematically in Fig. 2. Oscillations are generated by a driver system described in an earlier paper[10]. The test section is connected to the drivers by a rectangular plenum. The flow channel is at the top of the test section

and is a rectangular slot with an easily variable width h in the cross-stream direction y, a length L of 24.1 cm in the streamwise direction x, and a depth W of 15.2 cm in the spanwise direction into the plane of the page. Three interchangeable pairs of channel plates with edge radii $r = 0.64, 1.27$, and 2.54 cm are used. The walls on the spanwise sides of the test section are made of glass to allow flow visualization or optical measurements. In air at 80 kPa (Los Alamos atmospheric pressure), the apparatus can produce oscillating velocities up to 50 m/s, and has a frequency range of $7 < 1/T < 120$ Hz.

The flow is visualized using the double-pass shadowgraph technique[11]. The images are acquired phase locked to the driving signal with a 1000×1000-pixel 10-bit CCD camera. The necessary density gradients are generated by the addition of a small amount (less that 1% of the peak oscillating flow rate) of hydrofluorocarbon R134a introduced into the flow below the channel. The R134a is injected in a thin sheet, normally at the spanwise center of the plenum. Therefore, the resultant images should be interpreted similarly to dye or smoke sheet images.

Determination of acoustic power dissipation requires measurements of the time-varying pressure and a cross-stream average of velocity. Phase-locked velocities are measured on one cross-stream half of the slot using a single straight hot-wire probe mounted on a traverse that moves automatically from one measurement location to the next (Cross-stream symmetry has been confirmed). Spacing between locations is decreased near the wall to capture the large velocity gradients in the boundary layer. In all cases, 360 samples are acquired per cycle at each location, and the results are phase averaged over 250 cycles.

Oscillating flow is not a typical application of hot-wire anemometry and several unique issues must be addressed. Since the temperature inside the test section is not exactly matched to the room temperature (the drivers generate and leak some heat into the test section), it is necessary to simultaneously measure the time-varying temperature using a constant-current cold wire to correct the hot-wire data based on the measured temperature. Furthermore, since the flow is oscillatory, great care must be taken to ensure that the hot-wire sensor is not in the wake of its supporting probe body during the inward part of the

cycle. This is accomplished by using a standard boundary-layer probe (where the sensor is offset laterally from the probe body) and pitching the probe body to further remove it from the flow path. The single-sensor hot-wire probe is not capable of sensing flow direction, and therefore its use is limited to regions where the flow direction is known to be along x throughout the cycle. Since the flow might separate during the inward stroke for sharp-edged slots, creating a y component of the velocity near the edges during part of the cycle, only rounded slot edges are considered. All measurements are made at the top of the straight portion of the slot, i.e. the bottom of the slot edge radius (see Fig. 2), a location that we call the exit plane and define as $x = 0$. Because flow inward looks the same as flow outward to the probe, the hot-wire signal is a rectified sine wave for sinusoidal flow. Processing software detects the flow reversals and changes the velocity sign appropriately before phase averaging is performed. The result of this procedure is $u_a(y, t)$ shown in some figures below.

Since an assumption of two dimensional flow is necessary in this study, the spanwise uniformity of the flow was checked in a series of measurements with the traverse oriented in the spanwise direction. The flow at the exit plane was found to be spanwise uniform, save for the boundary layers on the spanwise edges. Fortunately, for oscillatory flow, it was found that the spanwise boundary layers have exactly the same thickness and shape as the cross-stream boundary layers which are measured as part of each data set. Therefore, the effect of the spanwise boundary layers on the average velocity can be easily accounted for.

An example of phase-averaged velocity results is shown in Fig. 3. Cross-stream profiles of the streamwise component of velocity are shown at eight points in time equal spaced through the full cycle. The profiles during the blowing stroke have a substantially thicker boundary layer than those for the suction stroke—the oscillatory boundary layer requires some streamwise distance to become established, and the entering inflow has not traversed such a distance. The accelerating flow ($t/T = 0.125$) tends to be laminar (as evidenced by the maximum near the wall) while the decelerating flow ($0.25 < t/T < 0.375$) is turbulent, as observed previously[12]. However, the profile of the turbulent oscillating flow deviates significantly from that of steady channel flow at a similar Reynolds number. Data from

Hussain and Reynolds[13] for a Reynolds number of 23,300 based on the centerline velocity and the half channel height are also shown in Fig. 3. Using a similar definition (and using the peak centerline velocity) the Reynolds number of the present data is 21,400. For steady flow, the centerline velocity is the peak of the profile and the velocity falls gradually toward the wall until the boundary layer is reached and the rate of decrease becomes much larger. However, for the oscillatory flow at $t/T = 0.25$, the velocity profile is flat at the centerline value for 80% of the channel.

Nonlinear effects in the driving system result in some distortion of the average-velocity waveform. These result in 2nd and 3rd harmonics that on average are 1% and 2% of the fundamental, respectively. We believe that this small departure from sinusoidal flow does not alter the flow physics. However, it would cause significant errors in the normalized pressure and acoustic power if not accounted for. Therefore, pressure and acoustic power are normalized separately over the blowing and suction strokes using the integrals of u_a^2 and U_a^3 where U_a is the volume flow rate at location a over each half of the cycle. Since we believe that this corrects the distortion, the data will be presented as if the flow were sinusoidal.

Pressure measurements are made simultaneously with the velocity measurements using a series of piezo-resistive pressure transducers mounted directly into the slot block walls at seven streamwise positions. In order to avoid errors caused by the small nonlinearity of these transducers[10], the full voltage waveforms from the transducers are digitized and a nonlinear calibration curve is used to convert voltages to pressures. Time-averaged pressure measurements upstream of $x = 0$ are extrapolated to obtain an exit-plane value.

Referring to Eqs. (3) and (4), we see that changes in pressure between two points can come from three sources: 1) conversion of kinetic energy to flow energy due to streamwise velocity differences, 2) minor losses, and 3) time-dependent inertial effects. The time-varying pressure difference between the various measurement stations and the ambient and volume flow rate measured at $x = 0$ are shown in Fig. 4 for a representative case. It should be noted that compressible effects upstream of $x = 0$ are small in all cases reported here, so the volume flow rate can be assumed independent of x inside the slot. The thin solid trace is

the pressure measured below the slot blocks. The velocities above and below the blocks are similar, so there is little contribution from kinetic energy conversion to the pressure below the blocks. Pressure oscillations are dominated by linear inertial effects in the slot, as is evident from the fact that the sinusoidal pressure leads the volume flow rate by almost 90°. The deviation from 90° is due to minor losses at both ends. In addition, the pressure amplitude is somewhat greater than the ordinary inertial pressure difference because of the minor losses (which generate pressure differences that are about half of the inertial pressure difference). Near the top of the slot ($x/h = -1.1$), the length of the slug of fluid between the pressure sensor and the ambient is small while the velocity is much larger than in the ambient, and thus the pressure trace reflects only the minor losses and kinetic-energy conversion. At the lower end of the slot (e.g. $x/h = -6.9$), the pressure fluctuations must accelerate all the slot fluid above this location and the resultant pressure trace is a mixture of all three of these effects.

IV. RESULTS

A. Flow Visualization

We begin with flow visualization. In Fig. 5, a series of instantaneous schlieren images acquired at 12 points in time equally spaced through the blowing cycle are shown for a case with $L_o/h = 20, r/h = 1.0$, and $Re = 634$. The image domain is $4.2h$ wide and $3.9h$ high. The marked fluid does not arrive in the visualized domain until $t/T = 0.2$. Shortly thereafter, a vortex pair is observed forming along the rounded walls of the slot edge. The locations of the vortex cores indicate that the flow has expanded considerably during the vortex pair formation process. Somewhat later in the cycle, the vortex pair leaves the exit plane and is convected downstream ($t/T = 0.276$). The turbulent vortex pair grows quickly, and a turbulent "starting jet" forms behind it[14]. A more subtle but surprising effect is the separation behavior near the exit radius during the latter part of the blowing stroke.

The detachment point that is initially near $x = 0$ moves abruptly to 45° around the exit radius on both sides of the slot after the start of the decelerating part of the blowing stroke ($t/T = 0.301$). The flow remains attached downstream of $x = 0$ for the remainder of the blowing stroke, although the images indicate significant fluctuations in the detachment point. As will be shown below, the attachment past $x = 0$ results in deceleration of the flow, pressure recovery, and a reduced minor loss coefficient.

B. Pressure

The effects of each of the three parameters on the time-averaged pressure difference between the slot and the infinite space will be examined by fixing two parameters and varying the third. Pressure is scaled such that the normalized value is equal to K_B if $K_S \approx 0$ [see Eq. (8)] and K_B is independent of time during the blowing stroke. For the sake of describing the pressure data, it will be assumed that the suction loss is indeed negligible, as justified by the large r/h values used here.

The effect of L_o/h on the time-averaged pressure will be examined first. For very small stroke length ($L_o/h < 0.01$) the oscillations do not cause separation on the outward stroke, and therefore K_B is expected to be very small. As the stroke length becomes very large, which for a fixed velocity amplitude is equivalent to a very small frequency, the oscillatory jet should approach steady-jet behavior, for which $K_B \approx 1$. These expectations are confirmed in Fig. 6a, where the dimensionless stroke length is varied with dimensionless radius and Reynolds number fixed (three different radii and two Reynolds-number cases are shown). These data verify that in every case the loss coefficient is small at low L_o/h and grows with L_o/h. In addition, the various cases demonstrate that the loss at a given stroke length is smaller for a larger dimensionless radius and larger Reynolds number. It is also evident that the Reynolds number has a very strong effect on $\partial K_B/\partial(L_o/h)$.

Similarly, the effect of the dimensionless radius is determined by fixing the Reynolds number at two values (nominally $Re = 658$ and 931) and the stroke length at $L_o/h = 30$.

In order to achieve the range of r/h shown, all three sets of slot blocks are used. The data are plotted in Fig. 6b, and several trends are apparent. The blowing loss decreases monotonically with r/h. In addition, the larger Reynolds number cases have smaller losses.

The small discontinuities between the various sets of data with matched Reynolds number indicate that an additional dimensionless parameter is affecting the results. There are two possibilities: the slot aspect ratio W/h, or the stroke length relative to the slot length, L_o/L. Future researchers may want to control these parameters more carefully. Since, as stated in Section III, spanwise uniformity at the exit was confirmed for a small-aspect-ratio case ($W/h = 6.7$), we conjecture that the increase in the loss for smaller aspect ratios can only be due to spanwise nonuniformity of the flow at $x > 0$. Flow visualization (not shown) confirms that the downstream flow expands more in the y direction in the spanwise center than at the spanwise edge during the blowing stroke. The slot length can impact the results only if $L_o/L > 1$ since the maximum entrance length over which an oscillatory flow can develop is L_o (the flow reverses after traversing this distance). For slots that are much shorter than L_o, the channel flow boundary layer will not develop fully. For most of the present data, including the cases in Fig. 6b, $L < L_o$. The cross-stream velocity profiles at the peak of the blowing ($t/T = 0.25$) for cases with identical r/h, L_o/h, and Re but different L_o/L are found to have only minor differences in their velocity profiles. Hence, It seems that oscillatory-flow entrance lengths are significantly less that L_o, although this is currently an open question and worthy of further study.

The Reynolds-number dependence is shown in Fig. 6c. As stated in the discussion of Fig. 6a above, smaller dimensionless stroke lengths result in smaller loss coefficients at fixed Reynolds number. While at very small Re the decrease of K_B is more than linear, it becomes linear at larger Re for each of the stroke lengths and Reynolds numbers considered here. The large variation in the blowing loss at small Re is likely due to changes in the velocity profile shape associated with the transition from laminar to turbulent flow. This transition has been reported to occur near $Re = 550$ for flow in smooth circular pipes[12]. Evidence for this hypothesis is provided by velocity profiles from two of the cases in Fig. 6c, shown in

Fig. 7. The higher-Re profile has a substantially thinner boundary layer than the smaller-Re case has. This can potentially affect the loss coefficient in two ways: 1) the larger departure from a uniform profile in the smaller-Re case will result in a larger loss coefficient for the same reason that it does for steady flow, as noted in Section I, and 2) the thicker boundary layer in the smaller-Re case will likely separate from the edge radius sooner and result in a smaller pressure recovery and a larger minor loss.

The latter effect can be seen in the pressure traces shown in Fig. 8. Pressure and velocity are shown for three cases, including two from Fig. 6c and an additional case with the smaller of these two Reynolds numbers, the same L_o/h, and a smaller r/h. The average velocities are nearly identical and sinusoidal. For the entire suction stroke and part of the blowing stroke, the pressures are also very similar. However, before the peak of the blowing stroke ($t/T = 0.25$), the effects of Re and r/h become apparent. For $r/h = 1$ and $Re = 905$ (Fig. 8a), there is a large pressure recovery [$p(t/T = 0.185)/(\rho u_{a,\max}^2/2) = -0.44$]. Reducing the Reynolds number to 634 results in a decrease in the pressure recovery [$p(0.190)/(\rho u_{a,\max}^2/2) = -0.38$, Fig. 8b]. The reduction of r/h from 1.0 to 0.625 results in even less pressure recovery.

An additional flow visualization study confirmed that a larger radius or a larger Reynolds number results in increased expansion of the exiting flow, and therefore a smaller normalized time-averaged pressure (and presumably a smaller blowing loss coefficient). As noted above, Reynolds number also affects the velocity profile shape, which in turn affects the kinetic energy flowing out of the channel. The profile-shape effect can be removed from the pressure data by using a velocity scale that is based on the cross-stream average of the square of velocity. However the application of a loss coefficient to predict ΔP would require knowledge of the velocity profile. Since future researchers may not know the profile shape, this approach has not been used for data presentation here. Nevertheless, using this velocity scale reveals that as r/h becomes small, the effect of Re is diminished. Therefore, for a sharp-edged exit, it is likely that the losses based on the profile-based velocity scale will be a function of L_o/h only.

C. Acoustic Power Dissipation and Effectiveness

By assuming that all of the power flowing past the exit is lost to viscous dissipation, the variations of the normalized acoustic power dissipation with each of the three parameters and over the same parameter space reported in Fig. 6 are shown in Fig. 9. The effect of L_o/h is shown in Fig. 9a. Most of the data collapse on a single curve with the exception of the case with the very large radius and small Re, which has more power dissipation than the rest, including other small-Re cases. Also of note is the behavior near $L_o/h = 7$. This value of stroke length was identified by Smith and Swift[15] as the boundary between time-averaged "jetting" behavior and reingestion of the vortex pairs generated during the blowing stroke. Clearly acoustic power dissipation increases as the reingestion process becomes more dominant (e.g., as L_o/h becomes smaller). It is also interesting to note that no such effect is detectable in the pressure data for the same cases shown in Fig. 6a.

In contrast to the time-averaged pressure, acoustic power dissipation is a weak function of r/h, as can be seen in Fig. 9b. In some parts of the parameter space, the behavior is not monotonic. It should be noted that a representative error for these data is ± 0.0025.

Acoustic power dissipation is shown in Fig. 9c to decrease with increasing Reynolds number. Data for identical L_o/h and similar r/h are more or less collapsed, as is to be expected given the weak r/h effects discussed above. It also appears that the sensitivity of the power dissipation to Re decreases for increasing stroke length for $20 \leq L_o/h \leq 50$.

As stated in Section I, minor losses can be used to create time-averaged pressure differences to block streaming motions or to convert oscillating flow to steady flow[16]. Ideally, we would create this time-averaged pressure difference with minimal acoustic power dissipation. It is natural to form an "effectiveness" parameter that is the ratio of the dimensionless time-averaged pressure difference to the dimensionless acoustic power dissipation:

$$\eta = \frac{2 + 8\Delta P/\rho u_{a,\max}^2}{\dot{E}/\rho A u_{a,\max}^2}. \tag{9}$$

Assuming loss coefficients that are constant during the blowing and suction parts of the cycle, $\eta = 3\pi$ when $K_B \gg K_S$[16].

Using the data from Figs. 6 and 9, η is plotted versus the same three dimensionless parameters in Fig. 10. These data demonstrate that the effectiveness decreases with increasing r/h or Re. It is shown above that increasing either of these parameters improves the pressure recovery during the outward motion. A lack of this recovery is responsible for the time-averaged pressure difference desirable in some applications, so it is no surprise that improved pressure recovery can have a detrimental effect on the effectiveness. One might expect that at sufficiently small Re (e.g. laminar flow), the effectiveness would increase with r/h since the dissipation due to the inward flow is reduced with no impact on the pressure recovery during the blowing part of the cycle. No evidence of this is found in the present data. Although the effectiveness increases with stroke length for small (laminar) Re, it is a very weak function of L_o/h at larger Reynolds numbers.

V. CONCLUSIONS

The effect of minor losses on the time-averaged pressure and acoustic power dissipation generated by oscillating flow in a rounded entrance/exit between a rectangular channel and an infinite space has been investigated experimentally. Both of these quantities are functions of three dimensionless parameters: $L_o/h, r/h$, and Re. Cases with very small dimensionless stroke lengths tend toward linear oscillatory behavior and cases with large stroke lengths tend toward steady jet flow. Increasing the exit radius reduces the adverse pressure gradient experienced by the exiting flow and allows the flow to expand more in the cross-stream direction near the exit, resulting in smaller losses. This effect can be enhanced by increasing the Reynolds number. The Reynolds number also governs the transition from laminar to turbulent flow. Laminar flow has a thicker boundary layer and thus has larger loss coefficients (due to the velocity scale) and less tendency to expand and recover pressure (which also results in larger losses). It is also found that nonlinear inertial effects

prevent one from making the necessary assumptions to use the equation for acoustic power dissipation to determine the blowing and suction loss coefficients separately. A parameter is defined that estimates the effectiveness of the sudden expansion for generating time-averaged pressure differences with minimal acoustic power dissipation. It is found that the effectiveness increases with decreasing r/h and Re, and increases with increasing L_o/h for laminar flow.

ACKNOWLEDGEMENTS

G. S. would like to acknowledge the financial support of the Division of Materials Science in DOE's Office of Science. B. S. was supported initially by Los Alamos National Laboratory LDRD funds and later by the V.P. for Research at USU. We would also like to thank Scott Backhaus for his patience and generosity through many hours of discussion.

REFERENCES

[1] G. W. Swift, D. L. Gardner, and S. Backhaus. Acoustic recovery of lost power in pulse tube refrigerators. *J. Acoust. Soc. Am.*, 105:711–724, 1999.

[2] S. Backhaus and G. W. Swift. A thermoacoustic-Stirling heat engine: Detailed study. *J. Acoust. Soc. Am.*, 107:3148–3166, 2000.

[3] E. Fried and I. E. Idelchik. *Flow Resistance*. Hemisphere Publishing Corporation, New York, 1989.

[4] R. S. Wakeland and R. M. Keolian. Influence of velocity profile nonuniformity on minor losses for flow exiting thermoacoustic heat exchangers. *J. Acoust. Soc. Am.*, 2002. to appear.

[5] P. J. Morris, S. Boluriaan, and C. M. Shieh. Computational thermoacoustic simulation of minor losses through a sudden contraction and expansion. 7th AIAA/CEAS Aeroacoustics Conference, paper 2001-2272, 2001.

[6] A. Petculescu and L. Wilen. Lumped-element technique for the measurement of complex density. *J. Acoust. Soc. Am.*, 110(4):1950–1957, 2001.

[7] L. Wilen, A. Petculescu, and G. Petculescu. Impedance measurements of stacks, regenerators and jet pumps. Proceedings of the 17th International Congress on Acoustics, Rome, Italy, 2001.

[8] J. K. Vennard. One-dimensional flow. In V. L. Streeter, editor, *Handbook of Fluid Dynamics*. McGraw-Hill, New York, 1961.

[9] B. R. Munson, D. F. Young, and T. H. Okiishi. *Fundamentals of Fluid Mechanics*. John Wiley and Sons, New York, 2nd edition, 1994. Figure 8.28.

[10] B. L. Smith and G. W. Swift. Measuring second-order time-averaged pressure. *J. Acoust. Soc. Am.*, 110(2):717–723, 2001.

[11] G. S. Settles. *Schlieren and Shadowgraph Techniques*. Springer, 2001. Figure 3.8.

[12] M. Ohmi, M. Iguchi, K. Kakehashi, and M. Tetsuya. Transition to turbulence and velocity distribution in an oscillating pipe flow. *Bulletin of the JSME*, 25:365–371, 1982.

[13] A. K. M. F. Hussain and W. C. Reynolds. Measurements in fully developed turbulent channel flow. *J. Fluids Eng.*, 97:568–580, 1975.

[14] M. Gharib, E. Rambod, and K. Shariff. A universal time scale for vortex ring formation. *J. Fluid Mech.*, 360:121–140, 1998.

[15] B. L. Smith and G. W. Swift. Synthetic jets at large Reynolds number and comparison to continuous jets. 31st AIAA Fluid Dynamics Conference, paper 2001-3030, 2001.

[16] G. W. Swift. *Thermoacoustics: a unifying perspective for some engines and refrigerators*. Acoustical Society of America, 2002.

FIGURE CAPTIONS

FIG. 1. Schematic of transition between a flow channel and an open space which exhibits entrance/exit flow losses. The loss coefficient during blowing is K_B and that during the suction is K_S.

FIG. 2. Schematic of test section. The top of the test section exits to ambient conditions.

FIG. 3. Profiles of the streamwise component of velocity at $x = 0$, at eight equal increments in time through a full cycle, for $L_o/h = 20$, $r/h = 1.0$, and $Re = 905$, ($Re_h = u_{a,\max}h/2\nu = 21,400$). The start of the cycle ($t/T = 0.0$) is defined as the first time step with the volume flow rate > 0. (●) $t/T = 0.0$, (■) $t/T = 0.125$, (⧫) $t/T = 0.250$, (▲) $t/T = 0.375$, (○) $t/T = 0.500$, (□) $t/T = 0.625$, (◊) $t/T = 0.750$, (△) $t/T = 0.875$, (⊞) data from Hussain and Reynolds[13] for 2-D steady channel flow with $Re_h = u_{cl}h/2\nu = 23,200$, where u_{cl} is the centerline velocity.

FIG. 4. Volume flow rate and pressure at various locations upstream of the exit plane for $L_o/h = 20, Re = 905, r/h = 1.0$. Volume flow rate (——), pressure at $x/h = -1.1$ (— —), $x/h = -2.1$ (– –), $x/h = -3.1$ (- - -), $x/h = -4.4$ (···), $x/h = -4.9$ (— · —), $x/h = -5.9$ (— – —), $x/h = -6.9$ (— · · · —), in plenum (—).

FIG. 5. Schlieren images taken at 12 equally-spaced phase-points during blowing cycle ($0.2 < t/T < 0.48$, $L_o/h = 20, Re = 634, r/h = 1.0$).

FIG. 6. Time-averaged pressure difference between $x = 0$ and the ambient as a function of (a) stroke length, (b) dimensionless radius with $L_o/h = 30$, and (c) Reynolds number. The dashed line at 1 is the result[16] if $K_B = 1$ and $K_S = 0$.

FIG. 7. Profiles of streamwise velocity at $t/T = 0.25$ for $L_o/h = 20, r/h = 0.833$, and (—) $Re = 416$, (- - -)$Re = 587$.

FIG. 8. Normalized cross-stream-average velocity and normalized pressure for $L_o/h = 20$ and a) $Re = 905, r/h = 1.0$, b) $Re = 634, r/h = 1.0$, and c) $Re = 645, r/h = 0.625$.

FIG. 9. Acoustic power as a function of (a) stroke length, (b) dimensionless radius with $L_o/h = 30$, and (c) Reynolds number. The dashed line at $1/3\pi$ is the result[16] if $K_B = 1$ and $K_S = 0$, and time-dependent inertial effects are ignored.

FIG. 10. The effectiveness η as a function of (a) stroke length, (b) dimensionless radius, and (c) Reynolds number. The dashed line indicates a value of 3π.

FIGURES

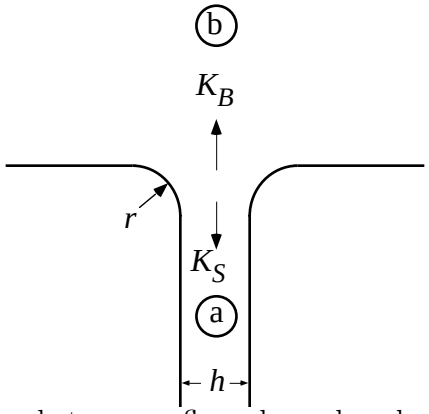

FIG. 1. Schematic of transition between a flow channel and an open space which exhibits entrance/exit flow losses. The loss coefficient during blowing is K_B and that during the suction is K_S.

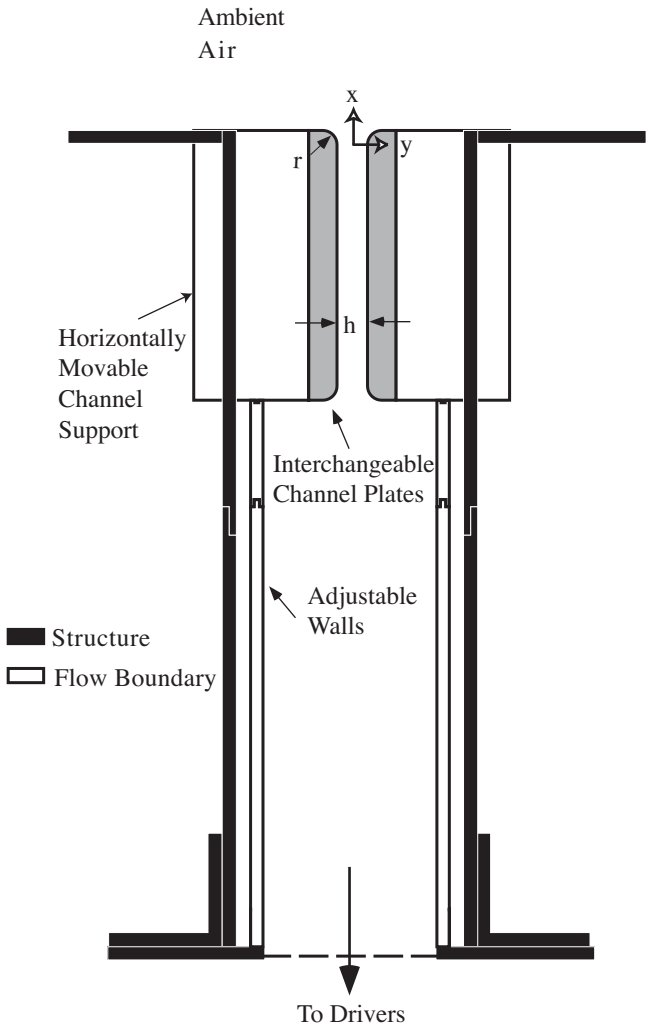

FIG. 2. Schematic of test section. The top of the test section exits to ambient conditions.

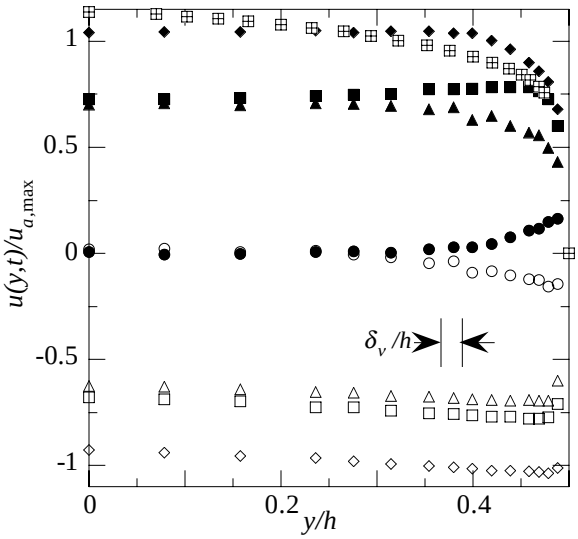

FIG. 3. Profiles of the streamwise component of velocity at $x = 0$, at eight equal increments in time through a full cycle, for $L_o/h = 20$, $r/h = 1.0$, and $Re = 905$, ($Re_h = u_{a,\max}h/2\nu = 21,400$). The start of the cycle ($t/T = 0.0$) is defined as the first time step with the volume flow rate > 0. ($\bullet$) $t/T = 0.0$, ($\blacksquare$) $t/T = 0.125$, ($\blacklozenge$) $t/T = 0.250$, ($\blacktriangle$) $t/T = 0.375$, ($\circ$) $t/T = 0.500$, ($\square$) $t/T = 0.625$, ($\lozenge$) $t/T = 0.750$, ($\triangle$) $t/T = 0.875$, ($\boxplus$) data from Hussain and Reynolds[13] for 2-D steady channel flow with $Re_h = u_{cl}h/2\nu = 23,200$, where u_{cl} is the centerline velocity.

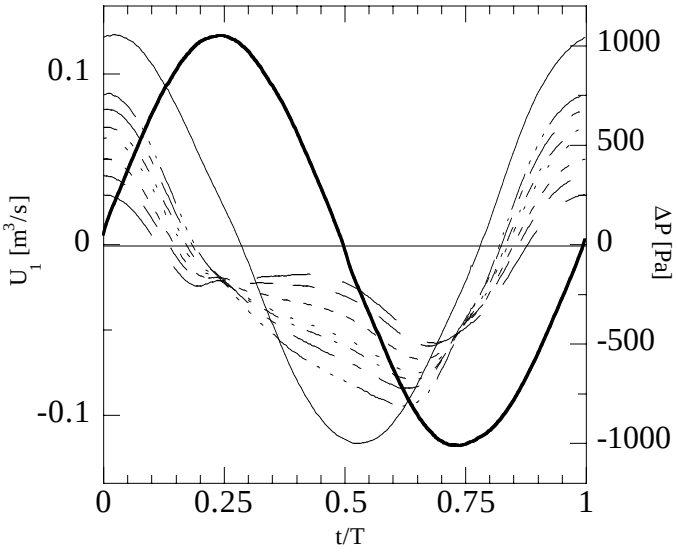

FIG. 4. Volume flow rate and pressure at various locations upstream of the exit plane for $L_o/h = 20, Re = 905, r/h = 1.0$. Volume flow rate (——), pressure at $x/h = -1.1$ (— —), $x/h = -2.1$ (– –), $x/h = -3.1$ (- - -), $x/h = -4.4$ ($\cdots$), $x/h = -4.9$ (— · —), $x/h = -5.9$ (— – —), $x/h = -6.9$ (— · · · —), in plenum (—).

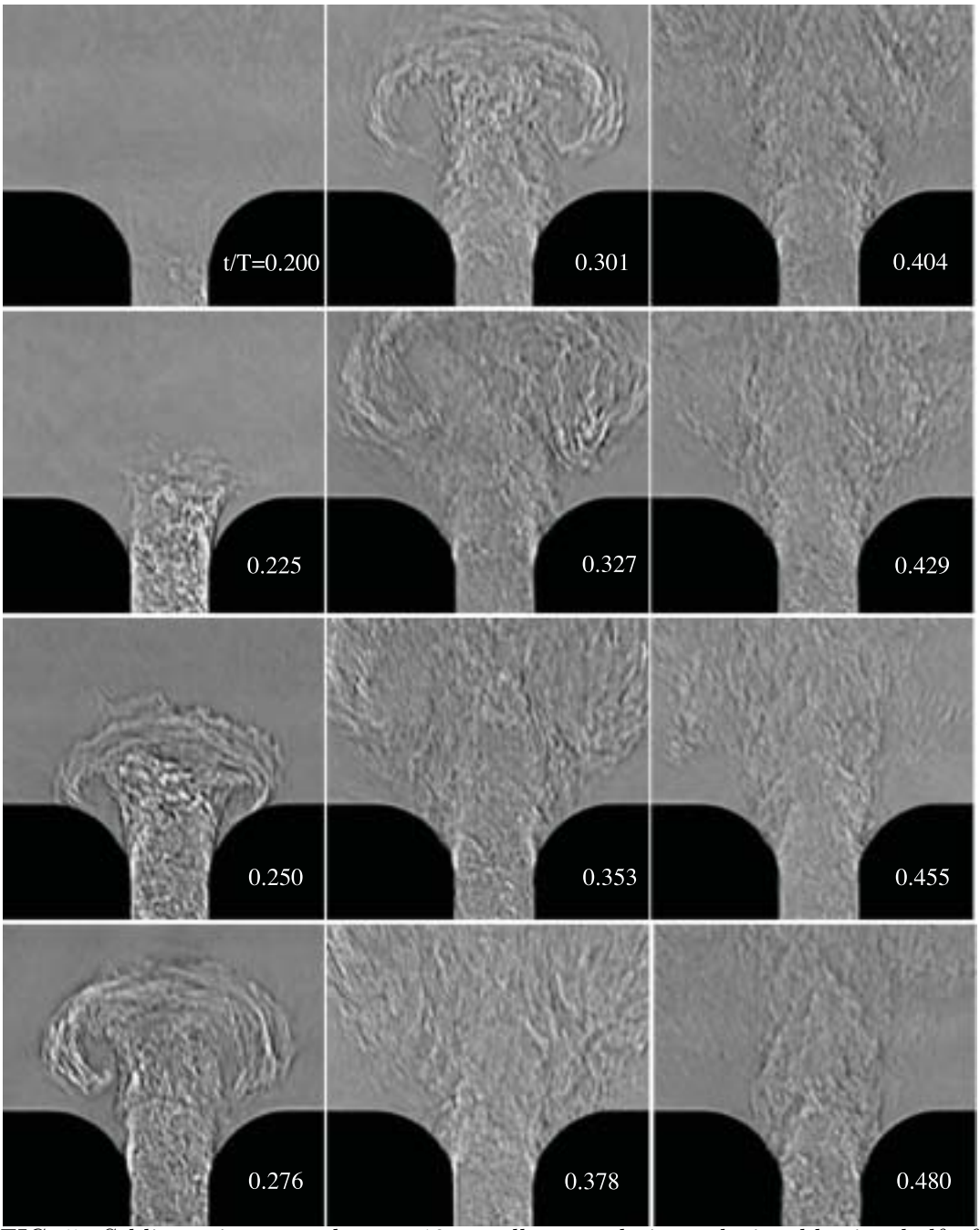

FIG. 5. Schlieren images taken at 12 equally-spaced times during blowing half of the cycle ($0.2 < t/T < 0.48$, $L_o/h = 20, Re = 634, r/h = 1.0$).

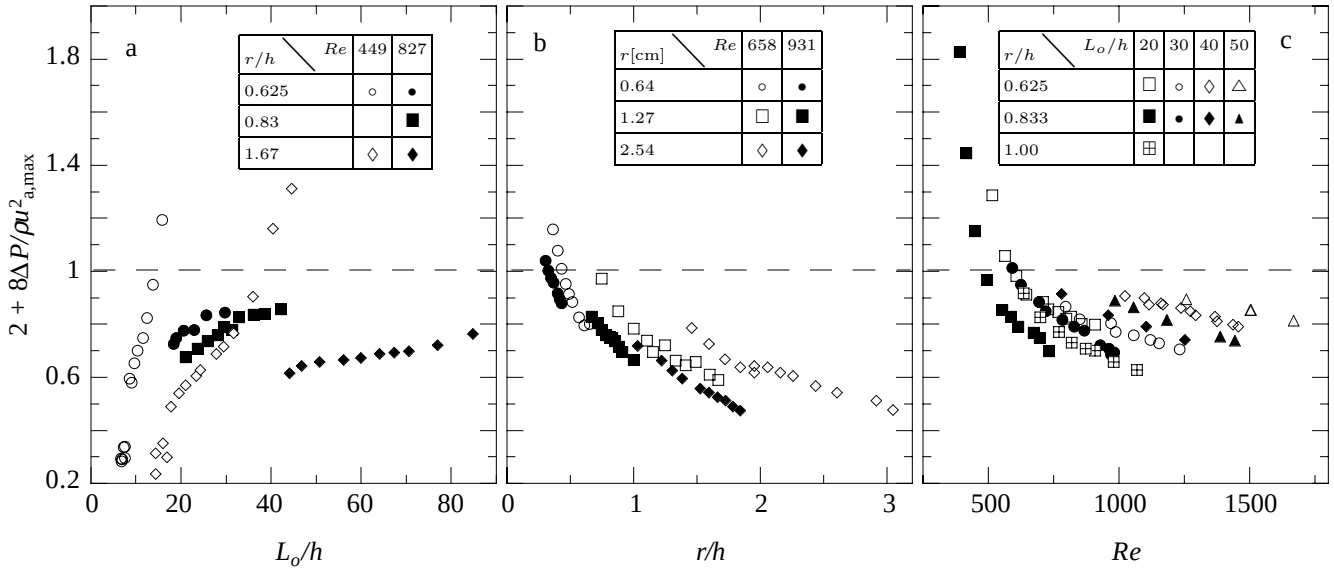

FIG. 6. Time-averaged pressure difference between $x = 0$ and the ambient as a function of (a) stroke length, (b) dimensionless radius with $L_o/h = 30$, and (c) Reynolds number. The dashed line at 1 is the result[16] if $K_B = 1$ and $K_S = 0$. The result would be zero if $K_B = K_S$.

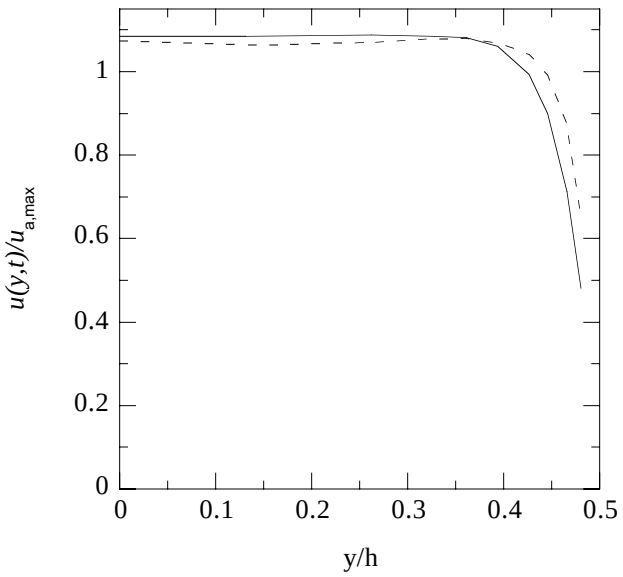

FIG. 7. Profiles of streamwise velocity at $t/T = 0.25$ for $L_o/h = 20, r/h = 0.833$, and (—) $Re = 416$, (- - -)$Re = 587$.

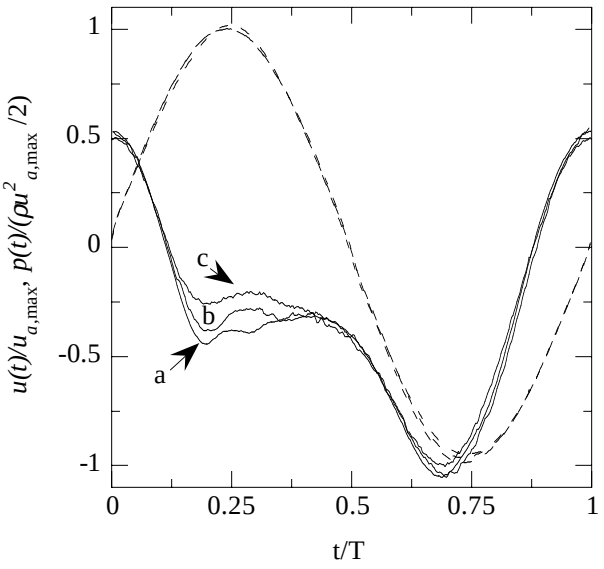

FIG. 8. Normalized cross-stream-average velocity and normalized pressure for $L_o/h = 20$ and a) $Re = 905, r/h = 1.0$, b) $Re = 634, r/h = 1.0$, and c) $Re = 645, r/h = 0.625$.

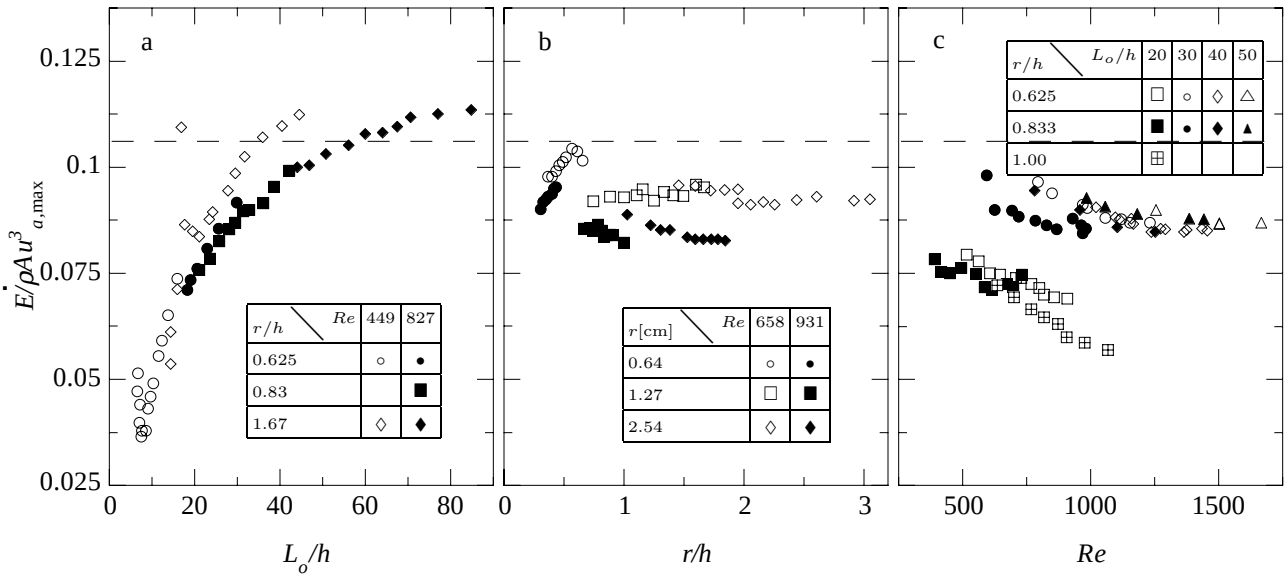

FIG. 9. Acoustic power as a function of (a) stroke length, (b) dimensionless radius with $L_o/h = 30$, and (c) Reynolds number. The dashed line at $1/3\pi$ is the result[16] if $K_B \gg K_S$, and time-dependent inertial effects are ignored.

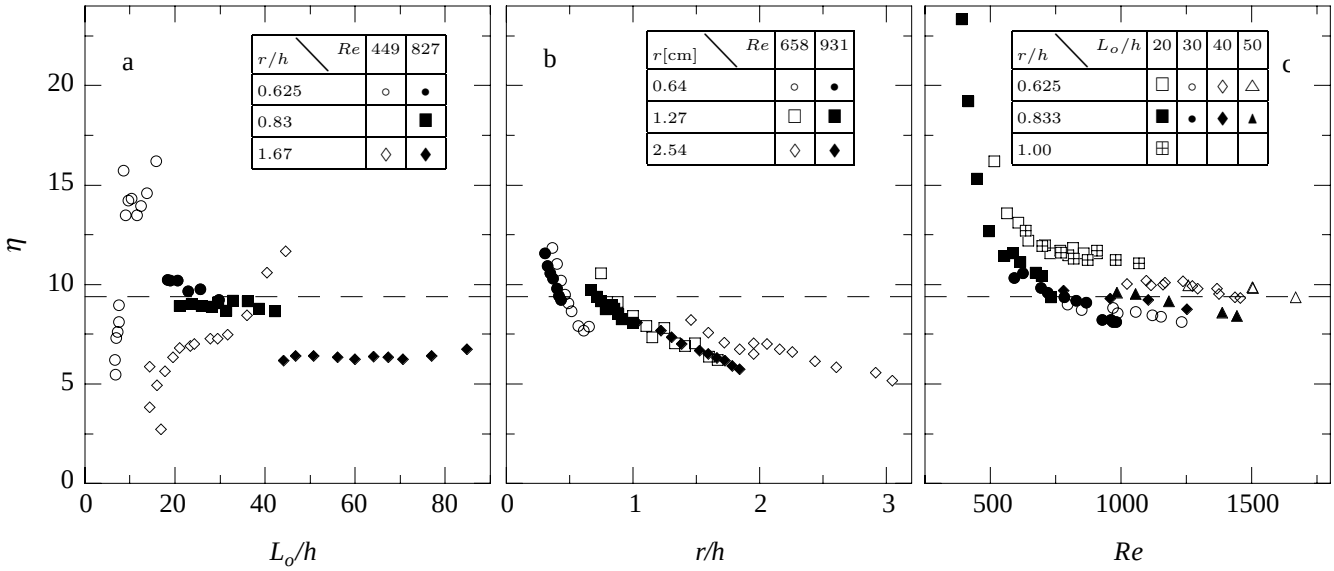

FIG. 10. The effectiveness η as a function of (a) stroke length, (b) dimensionless radius, and (c) Reynolds number. The dashed line indicates a value of 3π.